CrossMark

Scattering by PEC half-plane and disk placed on parallel planes

Mstislav E. Kaliberda[1] (ID), Leonid M. Lytvynenko[2] and Sergey A. Pogarsky[1]

[1]School of Radiophysics, Biomedical Electronics and Computer Systems, V.N. Karazin Kharkiv National University, Kharkiv, Ukraine and [2]Institute of Radio Astronomy of the National Academy of Sciences of Ukraine, Kharkiv, Ukraine

CAMBRIDGE
UNIVERSITY PRESS

Abstract

The scattering by the perfectly electric conducting (PEC) half-plane and PEC zero thickness disk placed on parallel planes is considered. The fields are represented in the spectral domain, i.e. in the domain of Fourier transform. The operator equations with respect to the Fourier amplitudes of the scattered field are obtained. The kernel functions of these equations contain poles. After regularization procedure, which is connected with the elimination of the poles, operator equations are converted to the system of singular integral equations. The convergence of the solution is based on the corresponding theorems. The scattered field consists of the plane wave, reflected by the infinite part of the half-plane, cylindrical waves, which appear as a result of scattering by the edge of the half-plane, and spherical waves, which appear as a result of scattering by the disk and multiple re-scattering by the disk-half-plane. The total near-field distribution and far-field patterns of cylindrical waves are presented.

Introduction

Circular disk and half-plane are canonical scattering objects. One can find classical solutions for scattering by the half-plane based on the method due to D. S. Jones, factorization of the kernel function of the dual integral equations and integral equations [1–5]. In [6], scattering of an arbitrary two-dimensional (2D) wave beam is analyzed. In [7], inhomogeneous plane wave and in [8] the Gaussian beam incidence is considered. In [8], special attention is paid to the shadow region. In [9], high-frequency asymptotic for the solution of scattering of an arbitrary 2D field is obtained. In [10, 11], the solution for the half-plane is used to obtain the asymptotic expressions for the antenna modeling.

The analysis of scattering by zero-thickness perfectly electric conducting (PEC) disk in free space or layered media with the guaranteed-convergent methods has represented an interesting electromagnetic problem for decades. In [12, 13], scattering by the circular disk or hole in the plane is considered with the method of moments. The Fourier amplitudes are expressed in terms of the series of hypergeometric polynomials, which are obtained as a result of integration of the Bessel functions. In [14, 15], the power series expansion and spheroidal wave function is used. In [16], the dual integral equations are obtained and solved with the use of the method of Kobayashi potentials.

In [17–19], one-dimensional electric-field integral equation in the scalar Hankel transform domain for the zero-thickness PEC circular patch resonator in multilayered media and zero-thickness PEC disk buried in a lossy half-space are discretized by means of Galerkin method.

In [20], scattering by an arbitrarily oriented zero-thickness PEC disk buried in a lossy half-space is formulated as electric-field integral equations in the vector Hankel transform domain and discretized with the use of Galerkin method. The matrix coefficients are converted to the rapidly converging integrals. In [21], the authors perform analytical regularization and discretization within one procedure, namely Galerkin projection on the set of judicious expansion functions, which are the eigenfunctions of the singular (static) part. The method of analytical regularization which leads to the Fredholm integral equation of the second kind is successfully applied to the analysis of the scattering by the finite-thickness thin PEC disk, dielectric disk, and graphene disk in [22–24]. The problem for the lens based on the disk inside the dielectric sphere excited by the dipole is reduced to the second-kind Fredholm matrix equation in [25].

Half-plane is an infinite object with an edge. From the mathematical point of view, it results in the appearance of poles in the kernel function of the integral equations. This requires the integration over contour in the complex plane. The edge can give us some interesting physical effects. For example, the PEC disk being not illuminated by the incident wave directly or being in the node of the standing wave can scatter the waves, which appear due to the edge of the half-plane.

In [26], we consider half-plane and disk placed on the same plane. In this paper, we consider plane wave scattering by PEC half-plane and disk in more general case, when they are placed on parallel planes. Here, an additional domain appears, a domain between the half-plane and the disk. From a mathematical point of view, this means that we need additional equations to describe the fields in this domain. From a methodological point of view, since the number of equations is increased as compared to [26], we need to introduce new operators which will allow us to write final equations in a concise form.

In this paper, we express scattered fields in the spectral domain in terms of the Fourier amplitudes (spectral functions), which are the Fourier transform of the currents density on the metal. The total scattered field can be represented as a sum of the fields of every isolated scatterer and the field which appears as a result of mutual coupling or re-scattering by the objects [27]. In case

components E_x and E_y. The incident field is

$$
\begin{pmatrix} E_x^i \\ E_y^i \end{pmatrix} = \begin{pmatrix} q_x \\ q_y \end{pmatrix} \exp\left(-ik(Ax + By + \gamma(A, B)z)\right) + \begin{pmatrix} p_x \\ p_y \end{pmatrix}
$$
$$
\times \exp\left(ik(Ax + By + \gamma(A, B)z)\right), \tag{1}
$$

where $k = 2\pi/\lambda$ is the wavenumber, $\gamma(A, B) = \sqrt{1 - A^2 - B^2}$ with Re $\gamma \geq 0$, Im $\gamma \geq 0$, $A = \cos\alpha$, $B = \cos\beta$, are cosines of the incident angles γ^1, α, and β with respect to the z, x, and y axis. The time dependence $\exp(-i\omega t)$ is omitted.

In the spectral domain, i.e. in the domain of Fourier transform, we seek scattered field as Fourier integrals with unknown amplitudes A_Θ, B_Θ, C_Θ, D_Θ, $\Theta = x, y$:

$$
E_\Theta^s(x, y) = \begin{cases} \int\limits_{-\infty}^{+\infty}\int\limits_{-\infty}^{+\infty} A_\Theta(\xi_x, \xi_y) \exp\left(ik(\xi_x x + \xi_y y + \gamma(\xi_x, \xi_y)z)\right)d\xi_x d\xi_y, & z > h, \\ \int\limits_{-\infty}^{+\infty}\int\limits_{-\infty}^{+\infty} (B_\Theta(\xi_x, \xi_y) \exp\left(ik\gamma(\xi_x, \xi_y)z\right) + C_\Theta(\xi_x, \xi_y) \times \exp\left(ik(\xi_y\Delta - \gamma(\xi_x, \xi_y)(z - h))\right) \\ \qquad \times \exp\left(ik(\xi_x x + \xi_y y)\right)d\xi_x d\xi_y, & 0 < z < h, \\ \int\limits_{-\infty}^{+\infty}\int\limits_{-\infty}^{+\infty} D_\Theta(\xi_x, \xi_y) \exp\left(ik(\xi_x x + \xi_y y - \gamma(\xi_x, \xi_y)z)\right)d\xi_x d\xi_y, & z < 0, \end{cases} \tag{2}
$$

the Fourier amplitudes of the field scattered by the isolated half-plane and the disk are known, or, in other words, their scattering operators are known, one can write operator equations for the scattered field of the whole structure. Since the kernel functions of these equations can have singularities in the form of poles of the integrands, some additional mathematical manipulations are needed to convert them to the solvable integral equations. The convergence of the solution is based on the corresponding theorems. This approach is successfully applied to the gratings of the infinite PEC or graphene screens in [28–30]. In [31], scattered fields consist of the fields of either plane waves or cylindrical waves, or both. Here, we are going to use this approach to the structure where scattered field consists of plane, cylindrical, and spherical waves. The rigorous solution for such a geometry is obtained for the first time. Potentially, it can be used in ring resonators and antenna design [32, 33], as well as to study the influence of the edge-effect.

Problem statement

Let us consider PEC half-plane $y < 0$, $z = 0$ and zero thickness PEC disk of radius r, $x^2 + (y - \Delta)^2 < r$, placed in the plane $z = h$, $h > 0$, where Δ is the shift of the disk along the y-axis. The plane wave with the Fourier amplitude $q = (q_x, q_y)^*$ is incident from the "upper" half-space $z > h$ and the plane wave with the Fourier amplitude $p = (p_x, p_y)^*$ is incident from the "lower" half-space $z < 0$, where "*" means transpose. Since we assume $h > 0$, to simulate the case of the disk placed below the half-plane, we introduce second incident wave with the Fourier amplitude p.

In the considered problem, all components of the electromagnetic field can be expressed via the independent tangential electric

The structure geometry and directions of wave propagation are shown in Fig. 1. Total field is the sum of the incident and scattered fields.

Let us introduce reflection and transmission operators of the isolated half-plane $y < 0$, $z = 0$, R_1, T_1, and disk $x^2 + y^2 < r$, which center coincides with the origin, R_2, T_2. Their action on arbitrary Fourier amplitude g is described by the integrals

$$
(R_j g)_\Theta(\xi_x, \xi_y) = \sum_{\Xi = x, y} \int\limits_{-\infty}^{+\infty}\int\limits_{-\infty}^{+\infty} R_{j,\Theta\Xi}(\xi_x, \xi_y, \zeta_x, \zeta_y)g_\Xi(\zeta_x, \zeta_y)d\zeta_x d\zeta_y, \tag{3}
$$

$$
(T_j g)_\Theta(\xi_x, \xi_y) = \sum_{\Xi = x, y} \int\limits_{-\infty}^{+\infty}\int\limits_{-\infty}^{+\infty} T_{j,\Theta\Xi}(\xi_x, \xi_y, \zeta_x, \zeta_y)g_\Xi(\zeta_x, \zeta_y)d\zeta_x d\zeta_y,
$$

$$
\Theta = x, y, \; j = 1, 2. \tag{4}
$$

Kernel functions of the scattering operators $R_{j,\Theta\Xi}(\xi_x, \xi_y, \zeta_x, \zeta_y)$, $T_{j,\Theta\Xi}(\xi_x, \xi_y, \zeta_x, \zeta_y)$ are supposed to be known. The reflection operators of the half-plane can be found by the factorization of the kernel of dual integral equations [5]. The reflection operators of the disk can be found by the method of moments [12, 13]. In [12, 13], the problem is considered only for case the wave vector of the incident field is in the plane XOZ, the scattered field is represented in the cylindrical coordinate system. The case of arbitrary incidence can be obtained with the use of the affine transformation of rotation. In our analysis, we need scattered fields to be represented in the Cartesian coordinate system as a superposition of the plane waves which propagate under real and complex angles. For this purpose, we use representation of the Bessel
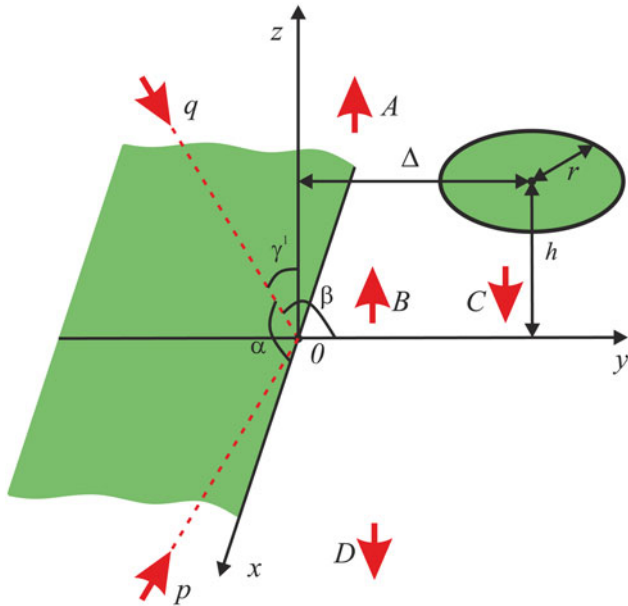
Fig. 1. Structure geometry.

function $J_m(x)$ in the form of superposition of plane waves:

$$J_m(x) = \frac{(-i)^m}{2\pi} \int_{\varphi - 2\pi}^{\varphi} \exp\left(i(x \cos \psi - m\psi)\right) d\psi.$$

Operator equations

As we have mentioned in the Introduction, scattered field can be represented as a sum of the field scattered by the isolated half-plane and the disk, and the field re-scattered by them. If we denote the Fourier amplitude of the field of re-scattered waves, which propagate to the positive direction of the z-axis as B, and which propagate to the negative direction of the z-axis as C (2), then one can write the following operator equations:

$$A = e^- s^- T_2 e^+ s^+ B + e^- s^- R_2 e^- s^+ q, \tag{5}$$

$$B = R_1 e^+ s^- C + T_1 p, \tag{6}$$

$$C = R_2 e^+ s^+ B + T_2 e^- s^+ q, \tag{7}$$

$$D = T_1 e^+ s^- C + R_1 p, \tag{8}$$

where action of the operators $s^\pm$ and $e^\pm$ is reduced to multiplication by $\exp(\pm i k \xi_y \Delta)$ and $\exp(\pm i k \gamma(\xi_x, \xi_y) h)$. They describe the phase variations if the coordinate system is shifted in the positive or negative direction of the y- and z-axis.

Let us notice first that reflection and transmission operators are connected as follows: $T_j = I + R_j$, $j = 1, 2$, where I is unit operator. Also let us subtract the Fourier amplitude of the incident plane wave (which is proportional to the delta-function) from the Fourier amplitude of the scattered field. Introduce new functions C_1, B_1 as follows:

$$B_1 = B - p, \quad C_1 = C - e^- s^+ q. \tag{9}$$

Then one can rewrite (5)–(8) as follows:

$$A = B_1 + e^- s^- R_2 e^+ s^+ B_1 + e^- s^- R_2 s^+ (e^+ p + e^- q), \tag{10}$$

$$B_1 = R_1 e^+ s^- C_1 + R_1 (p + q), \tag{11}$$

$$C_1 = R_2 e^+ s^+ B_1 + R_2 s^+ (e^+ p + e^- q), \tag{12}$$

$$D = e^+ s^- C_1 + R_1 e^+ s^- C_1 + R_1 (p + q) + p. \tag{13}$$

If C_1 and B_1 are determined from (11), (12), then from (10), (13) A and D also can be determined. Therefore, our purpose is to reduce (11) and (12) to solvable integral equations.

Integral equations

Kernel functions of the reflection operator of the half-plane have poles at the point which correspond to the propagation constant of the reflected plane wave. Kernel functions of the reflection operators of the half-plane and disk have integrable inverse square root singularity at the points which correspond to the waves which propagate along the XOY plane (sliding waves).

Let us represent the reflection operator of the disk as product of the singular and regular terms, also we subtract that part, which contains poles and gives plane wave in the reflected field. Introduce new functions which do not have singularities:

$$R_{2,\Theta,\Xi}(\xi_x, \xi_y, \zeta_x, \zeta_y) = R_{\Theta,\Xi}(\xi_x, \xi_y, \zeta_x, \zeta_y)\sqrt{1 - \xi_x^2 - \xi_y^2}, \tag{14}$$

$$B_{2,x}(\xi_x, \xi_y) = \left(B_{1,x}(\xi_x, \xi_y) + \frac{i}{2\pi} \frac{\sqrt{\sqrt{1 - A^2} - B}}{\sqrt{\sqrt{1 - A^2} - \xi_y}} \frac{q_x + p_x}{\xi_y - \underset{below}{B}}\right)$$
$$\times \sqrt{1 - \xi_x^2 - \xi_y^2}, \tag{15}$$

$$B_{2,y}(\xi_x, \xi_y) = \left(B_{1,y}(\xi_x, \xi_y) - \frac{i}{2\pi} \frac{A}{\sqrt{1 - A^2}}\right.$$
$$\times \frac{q_x + p_x}{\sqrt{\sqrt{1 - A^2} - B}\sqrt{\sqrt{1 - A^2} - \xi_y}}$$
$$\left. + \frac{i}{2\pi} \frac{\sqrt{\sqrt{1 - A^2} - \xi_y}}{\sqrt{\sqrt{1 - A^2} - B}} \frac{q_y + p_y}{\xi_y - \underset{below}{B}}\right)\sqrt{1 - \xi_x^2 - \xi_y^2}, \tag{16}$$

$$C_{2,\Theta}(\xi_x \xi_y) = C_{1,\Theta}(\xi_x, \xi_y)\sqrt{1 - \xi_x^2 - \xi_y^2}. \tag{17}$$

Notation "below" ("above") means that the poles should be bypassed from below (above). The Fourier amplitudes B_2 and C_2 describe only field of spherical waves.

After substitution of (14)–(17) as well as an explicit form of the reflection operator of the half-plane into (11), (12), one can obtain the integral equations. To write them in a more concise form first we introduce the following notations:

$$(F_1 g)(\xi_x, \xi_y) = \frac{i}{2\pi}\sqrt{\sqrt{1 - \xi_x^2} + \xi_y} \int_{-\infty}^{\infty} \frac{g(\xi_x, \zeta_y)}{\sqrt{\sqrt{1 - \xi_x^2} + \zeta_y}} \frac{d\zeta_y}{\zeta_y - \underset{below}{\xi_y}}, \tag{18}$$

$$(F_2 g)(\xi_x, \xi_y) = \frac{i}{2\pi} \sqrt{\sqrt{1 - \xi_x^2} + \xi_y} \int_{-\infty}^{\infty} \frac{g(\xi_x, \zeta_y)}{\sqrt{1 - \xi_x^2 - \zeta_y^2}} \frac{\xi_x}{\sqrt{1 - \xi_x^2}}$$

$$\times \frac{d\zeta_y}{\sqrt{\sqrt{1 - \xi_x^2} - \zeta_y}}, \tag{19}$$

$$(F_3 g)(\xi_x, \xi_y) = \frac{i}{2\pi} \sqrt{\sqrt{1 - \xi_x^2} - \xi_y} \int_{-\infty}^{\infty} \frac{\sqrt{\sqrt{1 - \xi_x^2} - \xi_y}}{\sqrt{\sqrt{1 - \xi_x^2} - \zeta_y}} \frac{g(\xi_x, \zeta_y)}{\sqrt{1 - \xi_x^2 - \zeta_y^2}}$$

$$\times \frac{d\zeta_y}{\underset{below}{\zeta_y - \xi_y}}, \tag{20}$$

$$F_4 g = \int_{-\infty}^{\infty} \int_{-\infty}^{\infty} \frac{g(\zeta_x, \zeta_y)}{\sqrt{1 - \zeta_x^2 - \zeta_y^2}} d\zeta_x d\zeta_y, \tag{21}$$

$$F_5 g = -\frac{i}{2\pi} \sqrt{\sqrt{1 - A^2} - B} \int_{-\infty}^{\infty} \frac{g(A, \zeta_y)}{\sqrt{\sqrt{1 - A^2} - \zeta_y}} \frac{d\zeta_y}{\underset{above}{\zeta_y - B}}, \tag{22}$$

$$F_6 g = \frac{i}{2\pi} \frac{A}{\sqrt{1 - A^2}} \frac{1}{\sqrt{\sqrt{1 - \alpha^2} - B}} \int_{-\infty}^{\infty} \frac{g(A, \zeta_y) d\zeta_y}{\sqrt{\sqrt{1 - \alpha^2} - \zeta_y}}, \tag{23}$$

$$F_7 g = -\frac{i}{2\pi} \int_{-\infty}^{\infty} \frac{\sqrt{\sqrt{1 - A^2} - \zeta_y} g(A, \zeta_y)}{\sqrt{\sqrt{1 - A^2} - B}} \frac{d\zeta_y}{\underset{above}{\zeta_y - B}}, \tag{24}$$

$$F_8 g = g(A, B). \tag{25}$$

Then integral equations are

$$B_{2,x} = F_1 e^+ s^- C_{2,x}, \tag{26}$$

$$B_{2,y} = F_2 e^+ s^- C_{2,x} + F_3 e^+ s^- C_{2,y}, \tag{27}$$

$$\begin{aligned} C_{2,\Theta} = &F_4 e^+ s^+ (R_{2,\Theta,x} B_{2,x} + R_{2,\Theta,y} B_{2,y}) + (q_x + p_x) F_5 e^+ s^+ R_{2,\Theta,x} \\ &+ (q_x + p_x) \cdot F_6 e^+ s^+ R_{2,\Theta,y} + (q_y + p_y) F_7 e^+ s^+ R_{2,\Theta,y} \\ &+ F_8 (R_{2,\Theta,x} s^+ (e^+ p_x + e^- q_x) + R_{2,\Theta,y} s^+ (e^+ p_y + e^- q_y)), \\ &\Theta = x, y. \end{aligned} \tag{28}$$

Integrands in (18), (20), (22), (24) have non-integrable singularities on the real axis. To eliminate the singularities the regularization procedure is needed.

Regularization procedure

To calculate integrals (18), (20), (22), (24) first we transform the integration path so that it coincides with the real axis everywhere except the pole. The pole is bypassed from above or below. Then we add and subtract such a function from the integrand that their sum has no singularities. The integral from this function itself can be calculated analytically. Taking into account that [34]

$$\int_{-\infty}^{\infty} \underset{below}{\frac{1}{\zeta - \xi}} d\zeta = \pi i, \tag{29}$$

$$\int_{-\infty}^{\infty} \underset{above}{\frac{1}{\zeta - \xi}} d\zeta = -\pi i, \tag{30}$$

obtain

$$\int_{-\infty}^{\infty} \underset{below}{\frac{g(\zeta)}{\zeta - \xi}} d\zeta = \int_{-\infty}^{\infty} \frac{g(\zeta) - g(\xi)}{\zeta - \xi} d\zeta + \pi i g(\xi), \tag{31}$$

$$\int_{-\infty}^{\infty} \underset{above}{\frac{g(\zeta)}{\zeta - \xi}} d\zeta = \int_{-\infty}^{\infty} \frac{g(\zeta) - g(\xi)}{\zeta - \xi} d\zeta - \pi i g(\xi). \tag{32}$$

Integrals on the right-hand side of (31), (32) are convergent. The integrands have no singularities. Thus we can understand them as Cauchy principal value integrals (notation *PV*). Taking into account that $PV \int_{-\infty}^{\infty} d\xi/\xi = 0$, finally obtain

$$\int_{-\infty}^{\infty} \underset{below}{\frac{g(\zeta)}{\zeta - \xi}} d\zeta = PV \int_{-\infty}^{\infty} \frac{g(\zeta)}{\zeta - \xi} d\zeta + \pi i g(\xi), \tag{33}$$

$$\int_{-\infty}^{\infty} \underset{above}{\frac{g(\zeta)}{\zeta - \xi}} d\zeta = PV \int_{-\infty}^{\infty} \frac{g(\zeta)}{\zeta - \xi} d\zeta - \pi i g(\xi). \tag{34}$$

Representation of (31), (32) in the form of Cauchy principal value integral (33), (34) is essential for us for discretization. In this case we can apply appropriate quadrature rule.

After regularization of (18), (20), (22), (24) as it is done in (33), (34), integral equations (26)–(28) can be discretized with the use of the quadrature rule. Equations (26)–(28) actually are the system of singular integral equations of the second kind on the infinite interval of integration.

Remark. In general, there is no need to explicitly express inverse square root singularity with the help of (14). However in this paper to solve integral equations (26)–(28) numerically we convert them to the system of algebraic equations with the help of quadrature rule. To build rapidly convergent discretization scheme, we should take into account singularities and thus to take proper quadratures.

For discretization of (26)–(28), we exchanged the infinite interval of integration by the bounded one $(-a; a)$. After that
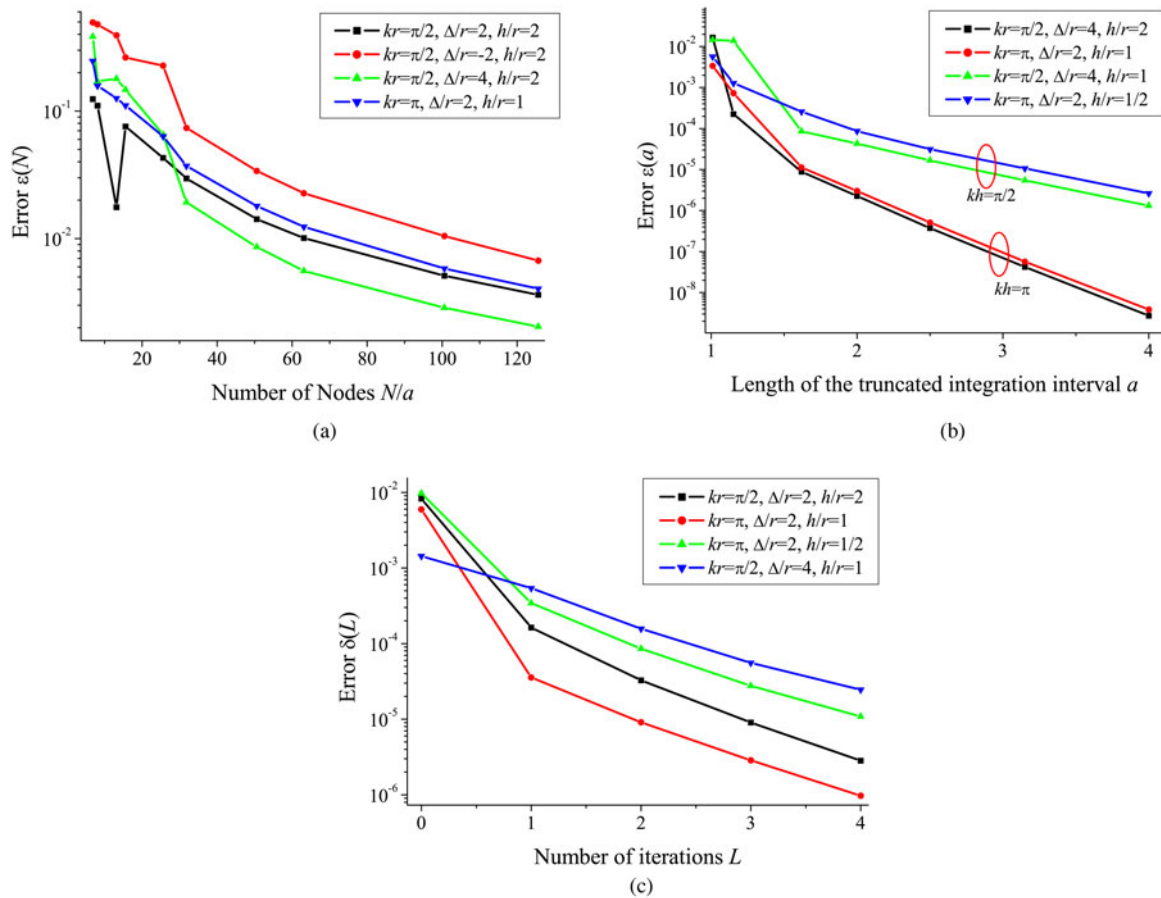
Fig. 2. Error of the solution: (a) $\varepsilon(N)$; (b) $\varepsilon(a)$; and (c) $\delta(L)$.

we divide segment $[-a; a]$ into N sub-segments and take single node point at the center of every sub-segment. Thus we use the compound midpoint rule for singular integrals.

After discretization, the linear matrix equation can be written as

$$\hat{B}_2 = M_1 \hat{C}_2, \tag{35}$$

$$\hat{C}_2 = M_2 \hat{B}_2 + q_x M_3 + p_x M_4, \tag{36}$$

where $\hat{B}_2$ and $\hat{C}_2$ are vectors which consist of unknown values of $B_{2,x}$, $B_{2,y}$, $C_{2,x}$, $C_{2,y}$ at the nodes, M_i, $i = 1, \ldots, 4$, are matrices and vectors which correspond to the right-hand side of (26)–(28) after discretization.

To solve (35), (36) we use the iterative procedure

$$\hat{C}_2^0 = q_x M_3 + p_x M_4, \tag{37}$$

$$\hat{B}_2^j = M_1 \hat{C}_2^j, \tag{38}$$

$$\hat{C}_2^{j+1} = M_2 \hat{B}_2^j + q_x M_3 + p_x M_4, \quad j = 0, 1, \ldots, L, \tag{39}$$

where superscript j means the number of iteration and L is the total number of iterations.

Numerical results

Let us study the convergence. Three parameters affect the error of the solution: number of nodes N, length of the truncated interval of integration a, and number of iterations L. We introduce error as follows:

$$\varepsilon(N) = |A^{sw}(N) - A^{sw}(2N - 1)|/|A^{sw}(2N - 1)|, \tag{40}$$

$$\varepsilon(a) = |A^{sw}(a) - A^{sw}(\Phi)|/|A^{sw}(\Phi)|, \tag{41}$$

$$\delta(L) = |A^{sw}(L) - A^{sw}(L + 1)|/|A^{sw}(L + 1)|, \tag{42}$$

where $A^{sw} = \sqrt{(A_x^{sw}(\xi_x = 0, \xi_y = 0))^2 + (A_y^{sw}(\xi_x = 0, \xi_y = 0))^2}$ is amplitude of the spherical wave in the orthogonal direction, $\Phi = 10$ is sufficiently large constant value.

The convergence of the presented scheme is based on the corresponding theorems about approximation of singular and regular integrals by quadrature rule [35]. However, the actual rate of convergence should be studied. Figure 2 shows dependences of the error on the number of interpolation nodes N, length of the interval of integration a, and the number of iterations L. Starting from the certain value of parameter, the convergence is monotone. Equations (26)–(28) contain exponentially decaying term, which is described by the operators $e^{\pm}$. As a result, $\varepsilon(a)$ decays
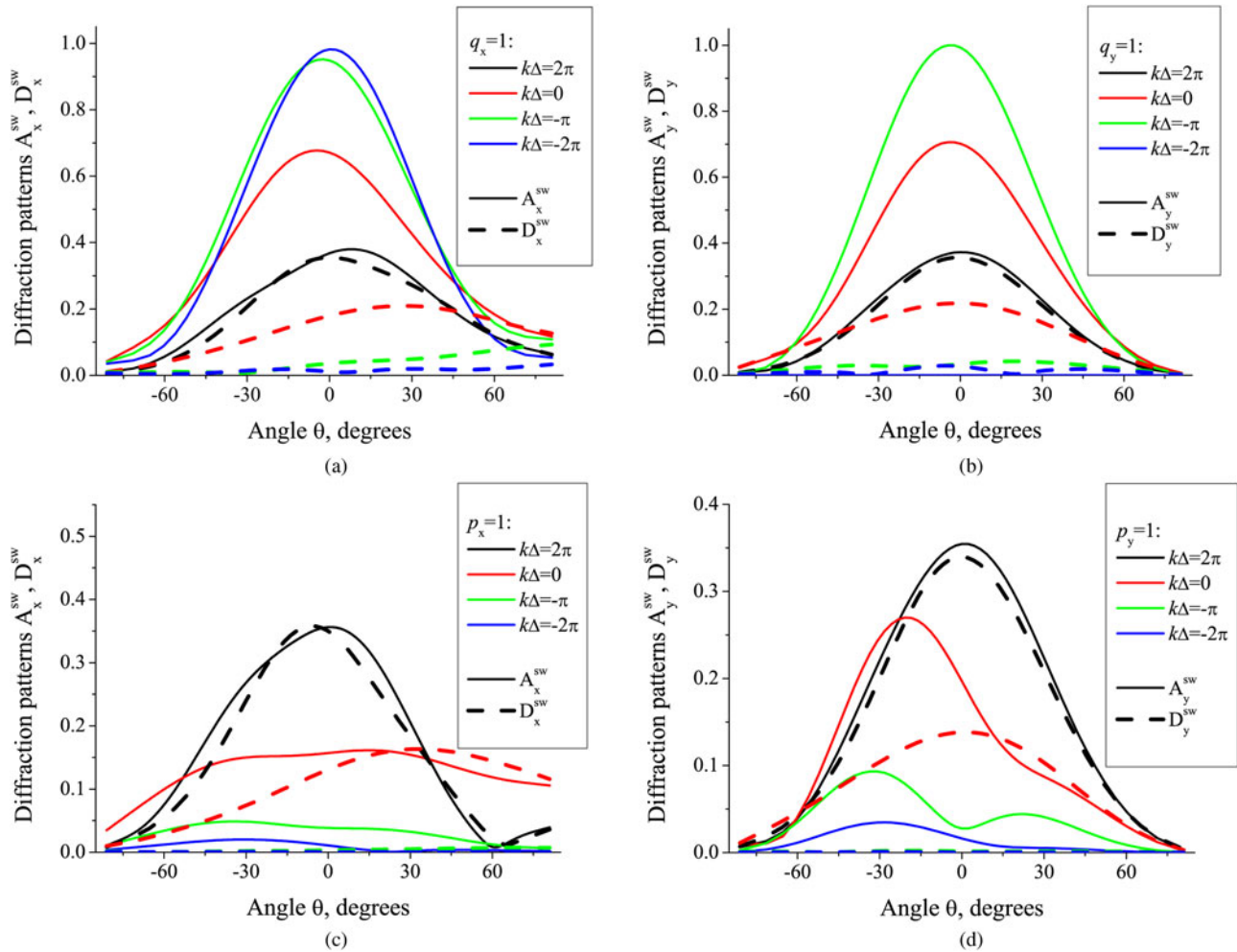
Fig. 3. Far-field patterns of spherical waves, non-zero electric-field components A_x^{sw} and A_y^{sw} (solid lines), D_x^{sw} and D_y^{sw} (dashed lines) for $k\Delta = 2\pi$ (black lines), $k\Delta = 0$ (red lines), $k\Delta = -\pi$ (green lines), $k\Delta = -2\pi$ (blue lines), $\varphi = 90^0$, $kr = \pi$, $kh = \pi/2$, normal incidence $\alpha = \beta = 90^0$: (a) $q_x \neq 0$, $q_y = p_x = p_y = 0$; (b) $q_y \neq 0$, $q_x = p_x = p_y = 0$; (c) $p_x \neq 0$, $q_x = q_y = p_y = 0$; and (d) $p_y \neq 0$, $q_x = q_y = p_x = 0$.

exponentially (see Fig. 2(c)), if $a \to \infty$. Here rate of convergence depends on kh. For larger values of kh, a faster convergence is observed.

Far field scattered by the structure can be represented as a sum of three summands:

$$E^{sc} = E^{pw} + E^{err} + E^{sw}, \qquad (43)$$

where E^{pw} is the field of the plane wave reflected (or transmitted) by the infinite part of the half-plane. It does not decay, if $k\rho \to \infty$, where ρ is the distance. The second summand in (43) E^{err} is expressed in terms of the error function. It describes the field of cylindrical waves except the plane $y = 0$, where it provides the continuity of the asymptotic representation of the far field. Finally E^{sw} is the field of spherical waves. It decays as $1/(k\rho)$, if $k\rho \to \infty$. It describes the mutual coupling of the half-plane and the disk, since E^{pw} and E^{err} are exactly the same as in the case of the isolated half-plane.

The saddle-point method gives us the expression for the diffraction patterns of the spherical waves with amplitudes A_Θ^{sw} (if

$z > 0$), D_Θ^{sw} (if $z < 0$)

$$|E_\Theta^{sw}(\rho \cos \phi \sin \theta, \rho \sin \phi \sin \theta)|$$

$$\sim \begin{cases} \dfrac{2\pi}{k\rho} A_\Theta^{sw}(\cos \phi \sin \theta, \sin \phi \sin \theta), & z > 0, \\[2mm] \dfrac{2\pi}{k\rho} D_\Theta^{sw}(\cos \phi \sin \theta, \sin \phi \sin \theta), & z < 0, \end{cases} \qquad (44)$$

where $\Theta = x$, y, (ρ, θ, ϕ) are coordinates of the spherical coordinate system, θ is the polar angle, φ is the azimuthal angle, A_Θ^{sw} and D_Θ^{sw} are that parts of the Fourier amplitudes A_Θ and D_Θ, which correspond to the spherical waves. They can be obtained from (10), (13) after regularization of integrals.

Figures 2–7 show far field of spherical waves. We study scattered fields for two values of the radius $kr = \pi/2$ ($r = \lambda/4$) and $kr = \pi$ ($r = \lambda/2$), two values of the distance between the plane and the disk along the z-axis $kh = \pi/2$ and $kh = \pi$, and several values of the shift Δ along the y-axis. The considered values of the radius correspond to the resonant cases. Near them the maxima and minima of the total scattering cross section of the isolated disk are observed [12]. All diffraction patterns are normalized by the global maximum. In the XZ plane, $\varphi = 0^0$, the
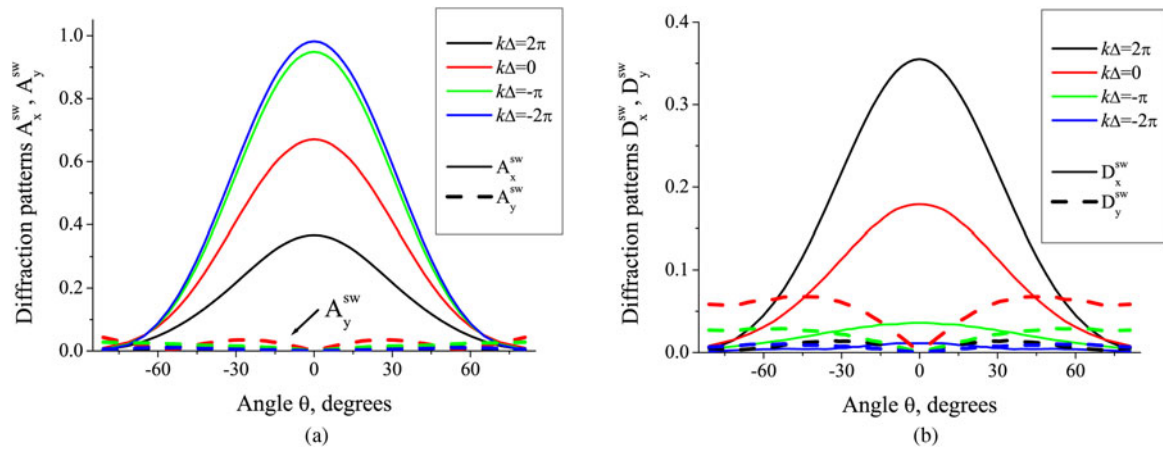
Fig. 4. Far-field patterns of spherical waves for $k\Delta = 2\pi$ (black lines), $k\Delta = 0$ (red lines), $k\Delta = -\pi$ (green lines), $k\Delta = -2\pi$ (blue lines) $\varphi = 0^0$, $kr = \pi$, $kh = \pi/2$, normal incidence $\alpha = \beta = 90^0$, $q_x \neq 0$, $q_y = p_x = p_y = 0$: (a) A_x^{sw} (solid lines), A_y^{sw} (dashed lines) and (b) D_x^{sw} (solid lines), D_y^{sw} (dashed lines).
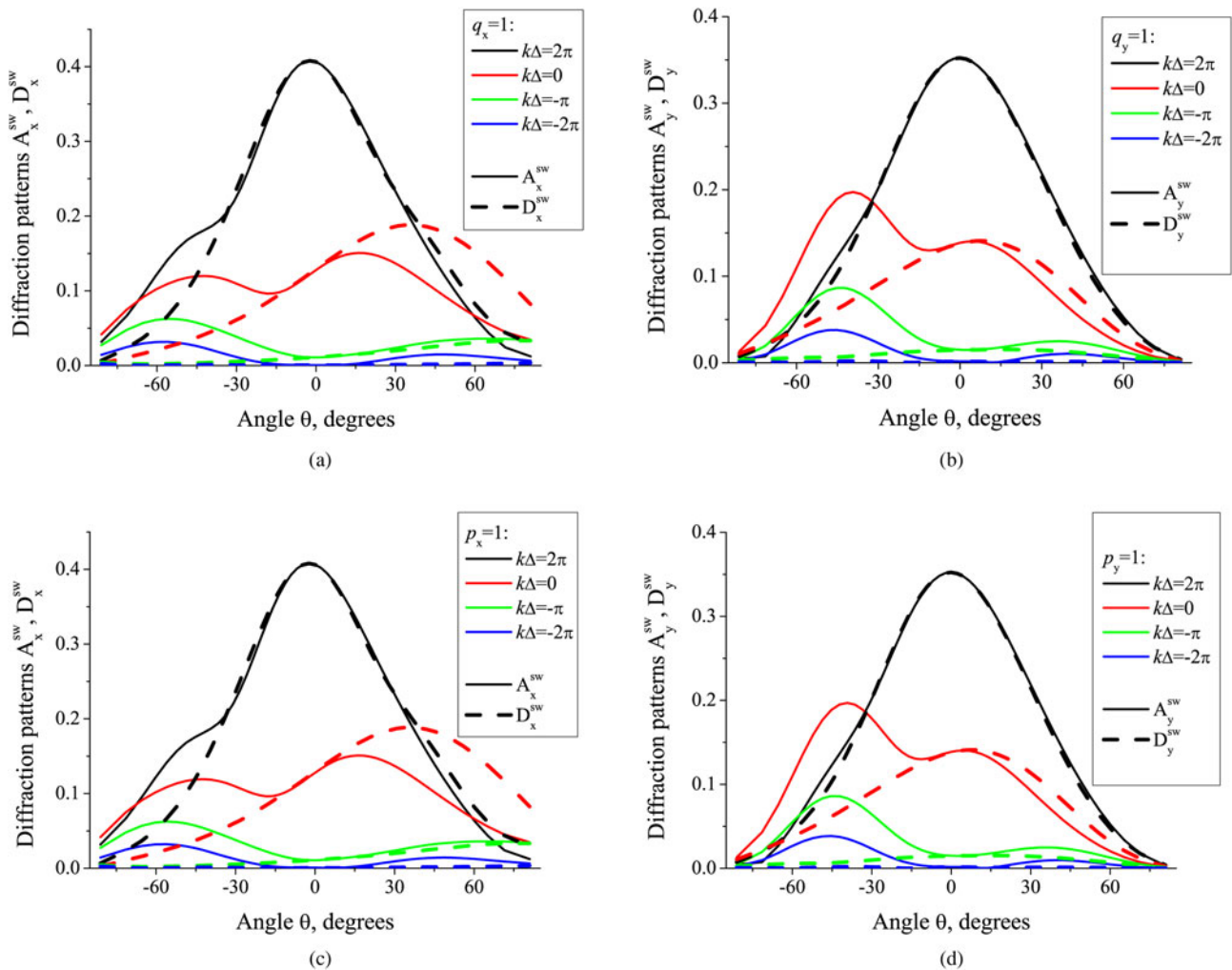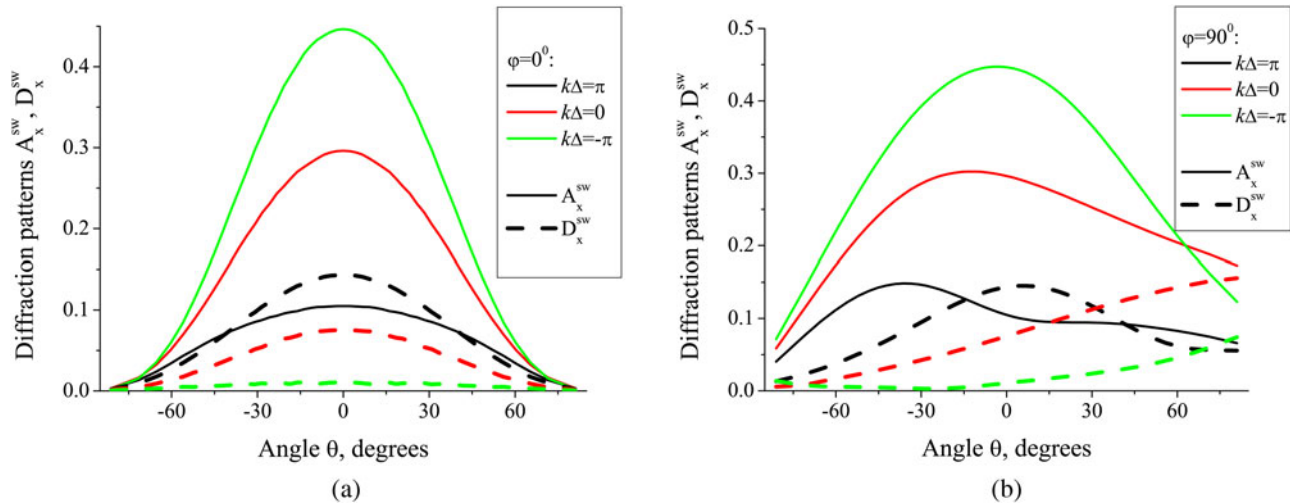

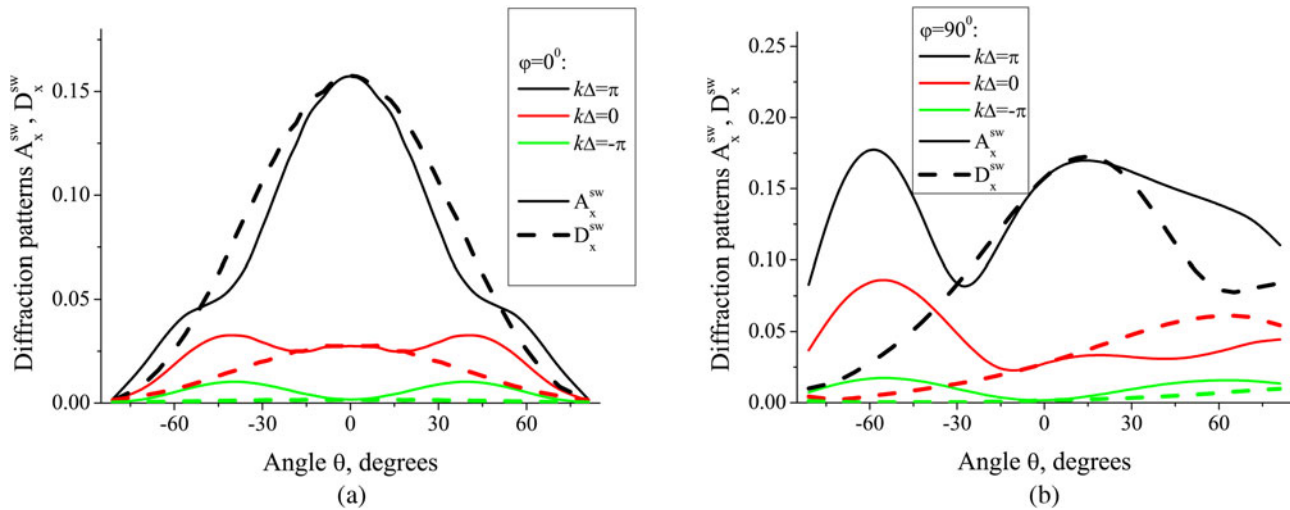**Fig. 5.** Same study as in Fig. 3, but for $kh = \pi$.

patterns are symmetric with respect to $\theta = 0^0$, since the structure is symmetric with respect to the y-axis.

In the case of the infinite PEC plane, value $kh = \pi/2$ corresponds to the maxima (hot-spot) and value $kh = \pi$ corresponds

to the minima (node) of the electric field of the standing wave formed by the superposition of the incident and reflected plane waves. In the case of infinite PEC plane, if we place PEC disk of zero thickness in the plane $kh = \pi$ there will be no scattering.

Fig. 6. Far-field patterns of spherical waves A_x^{sw} (solid lines), D_x^{sw} (dashed lines) for $k\Delta = \pi$ (black lines), $k\Delta = 0$ (red lines), $k\Delta = -\pi$ (green lines), $kr = \pi/2$, $kh = \pi/2$, normal incidence $\alpha = \beta = 90^0$, $q_x \neq 0$, $q_y = p_x = p_y = 0$: (a) $\varphi = 0^0$ and (b) $\varphi = 90^0$ (here $A_y^{sw} = D_y^{sw} = 0$).

Fig. 7. Same study as in Fig. 6, but for $kh = \pi$.

However, in our situation, in the case of the half-plane, non-zero field of cylindrical waves exists due to the presence of the edge. As a result, E^{sw} is also non-zero. At the same time, because of the presence of the standing wave, if $y < 0$, the amplitude of spherical waves for $kh = \pi/2$ (see Figs 3(a) and 3(b)) exceed the amplitude of spherical waves for $kh = \pi$ (see Figs 5(a) and 5(b)).

We study the scattered field for different shift Δ of the disk along the y-axis. For $\Delta > 0$, the disk is mainly placed in the field of the incident plane wave with small contribution of the field of the edge of the half-plane. The far-field shows almost the same behavior for $kh = \pi/2$ and $kh = \pi$. Consider first the case $q_x \neq 0$ or $q_y \neq 0$ (incidence from "above") and $p_x = 0$, $p_y = 0$. If one moves the disk toward the negative values of the y-axis, the far-field behavior significantly depends on the distance h. For $kh = \pi/2$, the disk is placed in the hot-spot of the standing wave. As a result, the amplitude of spherical wave growths toward some constant value when the influence of the cylindrical wave is neglected as compared to the standing wave. For $kh = \pi$, the

disk is placed in the node of the standing wave. As a result, the amplitude of spherical wave decreases if the disk is moved far from the edge of the half-plane, but $|E^{sw}| > 0$ due to excitation of cylindrical waves. In the case $p_x \neq 0$ or $p_y \neq 0$ (incidence from "below") the value of h does not influence significantly, since the disk is not illuminated by the plane wave at all for $\Delta < -r$.

Figures 8–10 show total field distribution in the vertical plane, $x = 0$, for different position of the disk. We consider the incidence from "above" (Figs 8 and 11) and from "below" (Figs 9 and 10). The patterns are normalized by the amplitude of the incident wave.

The reflected plane wave exists only in the domain $y < 0$. Except the rigorous theory, this is confirmed by the geometrical optics. The half-plane is the semi-infinite structure placed in the domain $y < 0$. Thus, in the domain $y < 0$ (in the case of orthogonal incidence) the plane wave is reflected, and in the domain $y > 0$ the plane wave is transmitted. The field of the
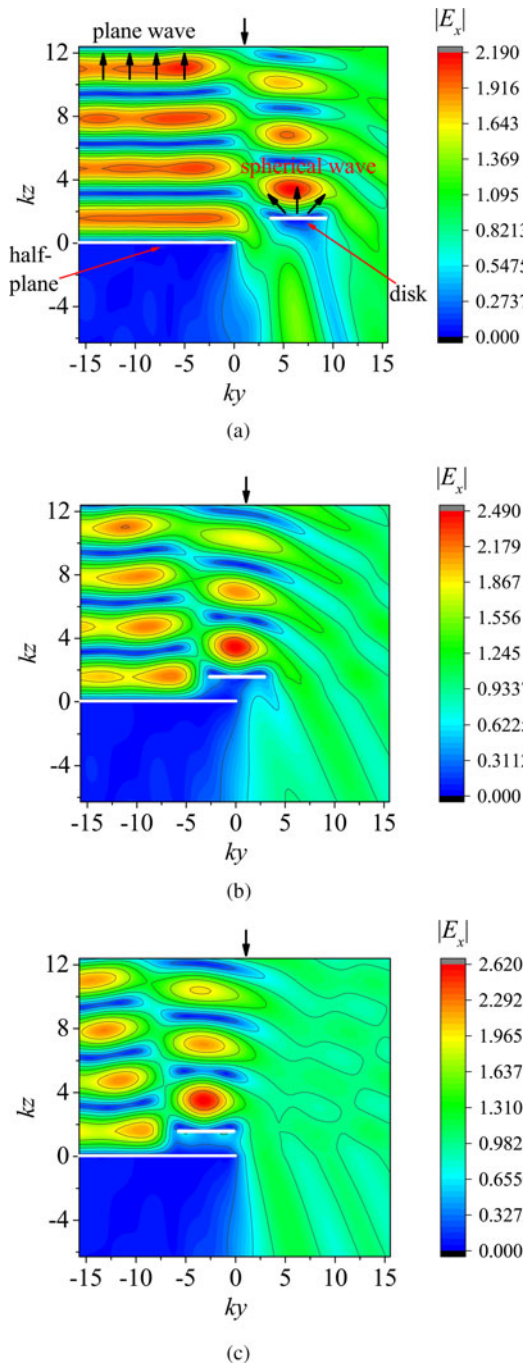
Fig. 8. Total field distribution $|E_x|$ in the plane $x = 0$ for $kr = \pi$, $kh = \pi/2$, $q_x \neq 0$, $q_y = p_x = p_y = 0$, normal incidence: (a) $k\Delta = 2\pi$; (b) $k\Delta = 0$; and (c) $k\Delta = -\pi$.

Fig. 9. Total field distribution $|E_x|$ for $x = 0$, $kr = \pi$, $kh = \pi/2$, $p_x \neq 0$, $q_x = q_y = p_y = 0$, normal incidence: (a) $k\Delta = 2\pi$; (b) $k\Delta = 0$; and (c) $k\Delta = -\pi$.

reflected plane wave in the domain $y < 0$ as well as the hot-spots at $kh = \pi/2 + \pi n$ and nodes at $kh = \pi n$, $n = 0, 1, 2, \ldots$ of the standing wave are clearly seen in Figs 8–10. Near the disk, the tangential components of the electric field vanish, $E_x = E_y = 0$. The minima of the tangential components of the electric field and spherical wave with hot-spots of the field near the disk are also seen in Figs 8–10.

Near the plane $y = 0$, the boundary between two domains appears: domain $y > 0$, where reflected plane wave does not exist, and domain $y < 0$, where reflected plane wave exists. The field scattered by the isolated half-plane at the boundary is described by E^{err} (see (43)). Plane $y = 0$ acts as a shadow boundary
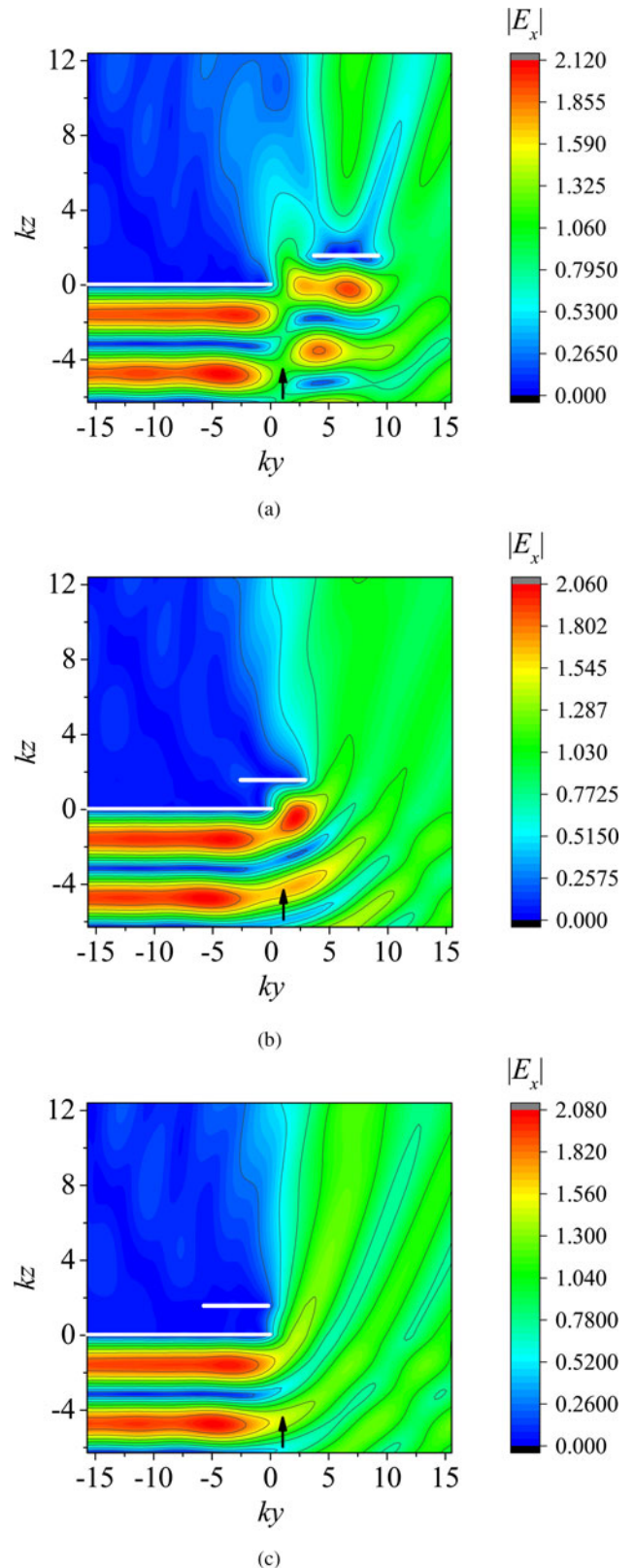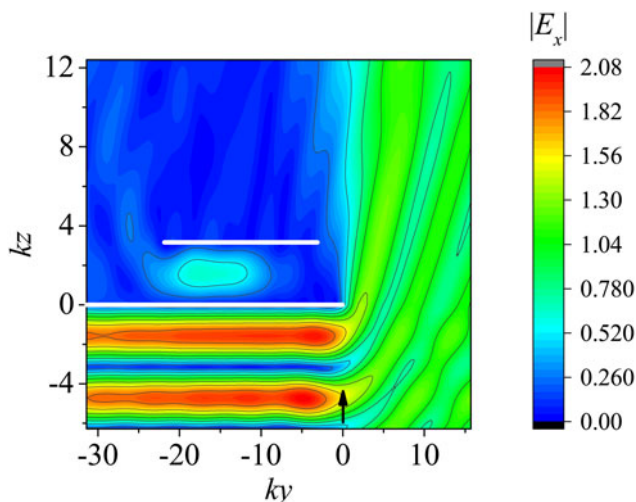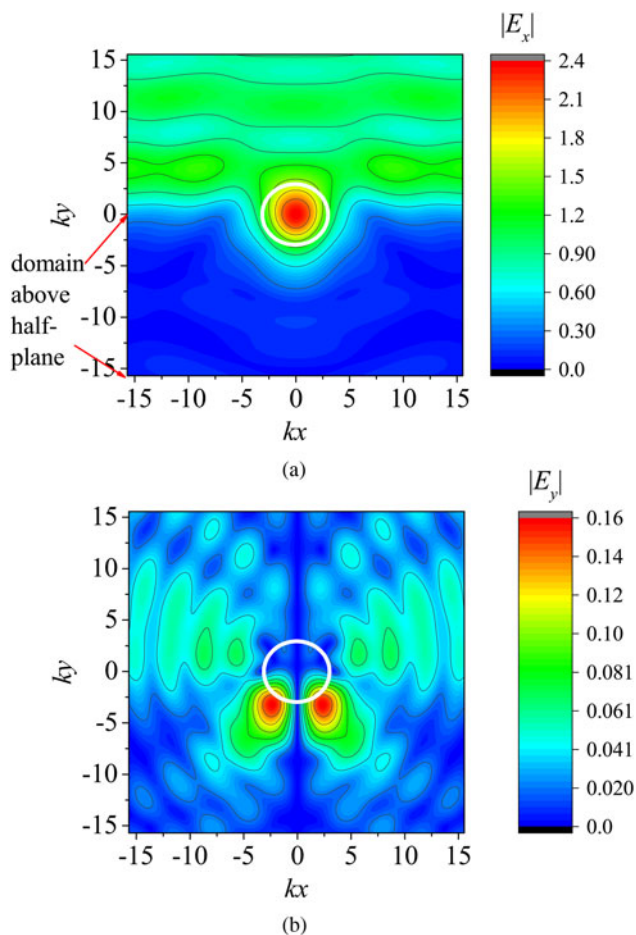
or transition region. The transition region also appears in other infinite structures with the edge, for example, in the semi-infinite strip gratings [31, 36].

Fig. 10. Total field distribution $|E_x|$ for $x = 0$, $kr = 3\pi$, $kh = \pi$, $p_x \neq 0$, $q_x = q_y = p_y = 0$, normal incidence.

Fig. 11. Total field distribution in the plane $z = 2h$ for $kr = \pi$, $kh = \pi/2$, $q_x \neq 0$, $q_y = p_x = p_y = 0$, normal incidence: (a) $|E_x|$ and (b) $|E_y|$.

For $\Delta < -r$, if $q_x = q_y = 0$ and $p_x = 1$, the disk is not illuminated by the plane wave, since it is situated totally "above" the half-plane (the incidence from "below"). Here, the disk is placed in the field of cylindrical wave excited as a result of scattering by the edge of

the half-plane. In Fig. 9(c), the field disturbance caused by the disk is slightly seen. Thus to illustrate better the field of the cylindrical wave scattered by the disk, in Fig. 10 we present pattern for lager value of the radius $kr = 3\pi$.

For full analysis, it is also necessary to show the field distribution in the horizontal plane. In Fig. 11 we present the near-field distribution in the plane $z = 2h$ ("above" the structure) which corresponds to the minimum of the amplitude of the standing wave. The graphs are symmetric with respect to the line $x = 0$, since the structure is symmetric. The field of the spherical wave is noticeable in the domain $y < 0$ especially for E_y. It is interesting to compare our results with results for an isolated disk (without half-plane). See, for example, [12]. In the case of the isolated disk in the plane perpendicular to $\vec{E}^i$ ($x = 0$), electric field has one maxima on the radius at the center of the disk.

Conclusion

In this paper, rigorous solution of the plane wave scattering by the circular PEC disk and PEC half-plane is obtained for the first time. The operator equations with respect to the Fourier amplitudes of the scattered field are reduced to the system of singular integral equations of the second kind. After discretization, the matrix equations are obtained, which are solved with the use of the iterative procedure.

The field scattered by the structure consist of plane wave, cylindrical waves, and spherical waves. The influence of the edge-effect of the half-plane on the disk is highlighted.

Conflict of interest. The authors declare none.

References

1. **Jones DS** (1950) Note on diffraction by an edge. *Quarterly Journal of Mechanics and Applied Mathematics* **3**, 420–434.
2. **Jones DS** (1952) A simplifying technique in the solution of a class of diffraction problems. *Quarterly Journal of Mathematics* **3**, 189–196.
3. **Noble D** (1958) *Methods based on the Wiener-Hopf Technique for the Solution of Partial Differential Equations.* London: Pergamon Press.
4. **Copson ET** (1946) On an integral equation arising in the theory of diffraction. *Quarterly Journal of Mathematics* **os-17**, 19–34.
5. **Copson ET** (1950) Diffraction by a plane screen. *Proceedings of the Royal Society of London* **202**, 277–284.
6. **Khestanov RK** (1968) Diffraction of a wave beam at a half-plane. *Radiophysics and Quantum Electrons* **11**, 793–799.
7. **Bertoni HL, Green A and Felsen LB** (1978) Shadowing an inhomogeneous plane wave by an edge. *Journal of the Optical Society of America* **68**, 983–989.
8. **Green AC, Bertoni HL and Felsen LB** (1979) Properties of the shadow cast by a half-screen when illuminated by a Gaussian beam. *Journal of the Optical Society of America* **69**, 1503–1508.
9. **Rahmat-Samii Y and Mittra R** (1978) Spectral analysis of high-frequency diffraction of an arbitrary incident field by a half plane – comparison with four asymptotic techniques. *Radio Science* **13**, 31–48.
10. **Gorobets NN, Yeliseyeva NP and Antonenko YA** (2012) Optimisation of radiation characteristics of wire-screened antennas. *Telecommunications and Radio Engineering* **71**, 59–69.
11. **Yeliseyeva NP, Gorobets AN, Katrich VA and Nesterenko MV** (2017) Radiation fields of a system of two impedance crossed vibrators excited in-phase and placed over a rectangular screen. *Progress in Electromagnetics Research B* **77**, 52503.
12. **Nomura Y and Katsura S** (1955) Diffraction of electromagnetic waves by circular plate and circular hole. *Journal of the Physical Society of Japan* **10**, 285–304.

13. **Lytvynenko LM, Prosvirnin SL and Khizhnyak AN** (1988) Semiinversion of the operator with the using of method of moments in the scattering problems by the structures consisting of the thin disks. Preprint institute of radio astronomy. *Academy of Sciences UKR SSR* **19**, 1–8 (in Russian).

14. **Bouwkamp CJ** (1950) On the diffraction of electromagnetic waves by small circular disks and holes. *Philips Research Reports* **5**, 401–422.

15. **Maixner J and Andrejewski W** (1950) Strenge Theorie der Beugung ebener elektromagnetischer Wellen an der vollkommen leitenden Kreisscheibe und an der kreisförmigen Öffnung im vollkommen leitenden ebenen Schirm. *Annalen der Physik* **442**, 157–168.

16. **Hongo K and Naqvi QA** (2007) Diffraction of electromagnetic wave by disk and circular hole in a perfectly conducting plane. *PIER* **68**, 113–150.

17. **Losada V, Boix RR and Horno M** (1999) Resonant modes of circular microstrip patches in multilayered substrates. *IEEE Transactions on Microwave Theory and Techniques* **47**, 488–498.

18. **Losada V, Boix RR and Horno M** (2000) Full-wave analysis of circular microstrip resonators in multilayered media containing uniaxial anisotropic dielectrics, magnetized ferrites, and chiral materials. *IEEE Transactions on Microwave Theory and Techniques* **48**, 1057–1064.

19. **Losada V, Boix RR and Medina F** (2003) Fast and accurate algorithm for the short-pulse electromagnetic scattering from conducting circular plates buried inside a lossy dispersive half-space. *IEEE Transactions on Geoscience and Remote Sensing* **41**, 988–997.

20. **Di Murro F, Lucido M, Panariello G and Schettino F** (2015) Guaranteed-convergence method of analysis of the scattering by an arbitrarily oriented zero-thickness PEC disk buried in a lossy half-space. *IEEE Transactions on Antennas and Propagation* **63**, 3610–3620.

21. **Lucido M, Panariello G and Schettino F** (2017) Scattering by a zero-thickness PEC disk: a new analytically regularizing procedure based on Helmholtz decomposition and Galerkin method. *Radio Science* **52**, 2–14.

22. **Balaban MV, Sauleau R, Benson TM and Nosich AI** (2009) Dual integral equations technique in electromagnetic wave scattering by a thin disk. *PIER B* **16**, 107–126.

23. **Lucido M, Balaban MV and Nosich AI** (2021) Plane wave scattering from thin dielectric disk in free space: generalized boundary conditions, regularizing Galerkin technique and whispering gallery mode resonances. *IET Microwaves, Antennas & Propagation* **15**, 1159–1170.

24. **Balaban MV, Shapoval OV and Nosich AI** (2013) THz wave scattering by a graphene strip and a disk in the free space: integral equation analysis and surface plasmon resonances. *IOP Journal of Optics* **15**, 114007/9.

25. **Tikhenko ME, Radchenko VV, Dukhopelnykov SV and Nosich AI** (2021) Radiation characteristics of a double-layer spherical dielectric lens antenna with a conformal PEC disk fed by on-axis dipoles. *IET Microwaves, Antennas & Propagation* **15**, 1249–1269.

26. **Kaliberda M, Lytvynenko L and Pogarsky S** (2022) Electromagnetic wave scattering by half-plane and disk placed in the same plane or circular hole in half-plane. *Journal of Electromagnetic Waves and Applications.* doi: 10.1080/09205071.2022.2032379.

27. **Schwarzschild K** (1901) Die beugung und polarisation des lichts durch einen. Spalt I. *Mathematische Annalen* **55**, 177–247.

28. **Kaliberda ME, Litvinenko LN and Pogarsky SA** (2010) Diffraction of H0m and E0m modes by a system of axially symmetric discontinuities in a coaxial circuit. *Journal of Communications Technology and Electronics* **55**, 505–511.

29. **Kaliberda ME, Lytvynenko LM, Pogarsky SA and Roiuk MP** (2018) Diffraction of the *H*-polarized plane wave by a finite layered graphene strip grating. *International Journal of Microwave and Wireless Technologies* **11**, 326–333.

30. **Kaliberda ME, Litvinenko LN and Pogarsky SA** (2021) Operator method in the problem of the *H*-polarized wave diffraction by two semi-infinite gratings placed in the same plane. *Radio Physics and Radio Astronomy* **26**, 350–357.

31. **Kaliberda M, Litvinenko L and Pogarsky S** (2017) Method of singular integral equations in diffraction by semi-infinite grating: *H*-polarization case. *Turkish Journal of Electrical Engineering Computer Sciences* **25**, 4496–4509.

32. **Zhang L, Yang J, Fu X and Zhang M** (2013) Graphene disk as an ultra compact ring resonator based on edge propagating plasmons. *Applied Physics Letters* **103**, 163114.

33. **Saidoglu NY and Nosich AI** (2020) Method of analytical regularization in the analysis of axially symmetric excitation of imperfect circular disk antennas. *Computers & Mathematics with Applications* **79**, 2872–2884.

34. **Muskhelishvili NI** (1972) *Singular Integral Equations. Boundary Problems of Functions Theory and their Applications to Mathematical Physics.* Groningen, The Netherlands: Wolters-Noordhoff (Revised translation from Russian).

35. **Lifanov IK** (1996) *Singular Integral Equations and Discrete Vortices.* Utrecht, The Netherlands: VSP.

36. **Hills NL and Karp SN** (1965) Semi-infinite diffraction gratings–I. *Communications on Pure and Applied Mathematics* **18**, 203–233.

Mstislav E. Kaliberda received his B.S. and M.S. degrees in Applied Mathematics from the V.N. Karazin Kharkiv National University, Kharkiv, Ukraine in 2005 and 2006, respectively, and his Ph.D. degree in 2013 from the same university. Now, he is an Associate Professor in the School of Radio Physics. His current research interests are analytical and numerical techniques, integral equation, multi-element periodic structures, and graphene gratings.

Leonid M. Lytvynenko graduated from the V.N. Karazin Kharkiv National University, Kharkiv, Ukraine and received the combined B.S. and M.S. degree in Radiophysics and Electronics in 1959 and his Ph.D. degree in 1965. From 1966 to 1985 he was with the Institute of Radiophysics and Electronics of the National Academy of Sciences of Ukraine (IRE NASU) in Kharkiv, Ukraine. He is Professor in Radiophysics since 1977. In 1985, he founded the Institute of Radio Astronomy of NASU and served as its Director until 2017. His area of research is in the theory of waves scattering and propagation, antenna systems and engineering, microwave sources, and radio astronomy. He is vice-chairman of the Ukrainian National URSI Committee, member of the European Astronomy Society, and member of the International Astronomy Society. He is also the editor-in-chief of the journal "Radio Physics and Radio Astronomy."

Sergey A. Pogarsky received his M.S. degree in Radiophysics and Electronics from the V.N. Karazin Kharkiv National University, Kharkiv, Ukraine in 1977, and his Ph.D. degree from the same university in 1984. Since 1977 he has been with the same university as researcher, and since 1984 as senior researcher and part-time senior lecturer at the Department of Physics of Ultra High Frequencies. Since 1999, he is Professor, and part-time Principal Scientist. His research interests include CAD techniques for microwave and millimeter wave components, antenna systems, and microwave transmission lines and circuits.